6.2 RELEASES OF PRESSURIZED LIQUEFIED GASES: SIMULATIONS OF THE DESERT TORTOISE TEST SERIES WITH THE CFD MODEL FLACS

Mathieu Ichard *[Φ], Olav Roald Hansen[#] and Jens Melheim*
[Φ] University of Bergen, Norway
*GexCon AS, Bergen, Norway
GexCon US, Bethesda, MD,USA

1. INTRODUCTION

Most Toxic Industrial Chemicals; chlorine, sulfur-dioxide, ammonia, etc., are stored and transported in urban areas in very large quantities as pressurized liquefied gases. The two factors, very large quantities and low normal boiling point, greatly enhance the hazards associated with such materials. Due to their low normal boiling point, they rapidly change phase and vaporize as they are released into the atmosphere. The violent vaporization, termed flashing, shatters the liquid jet and the material disperses as a two-phase jet in the atmosphere. In this first stage, the dispersion process is controlled by the source conditions and the momentum of the two-phase jet. A certain fraction of liquid aerosols can deposit on the ground leading to the formation of a pool which gradually evaporates. This deposition, referred to as rain-out in the following, has two opposite effects: it reduces the gas concentration that one can observe downwind of the release point by removing mass from the jet and it increases the duration of the hazard as gas evaporates from the pool for a long period after the release has stopped. In the second stage, all the liquid droplets have evaporated or they have been removed from the jet by the rain-out process. The initial high momentum of the jet has dissipated and the dispersion is controlled by atmospheric turbulence.

In our methodology, the whole chain of events involved in a pressurized liquefied gas release is modeled. The source term at the exit orifice where the flashing phenomenon occurs is estimated by using a 1D expansion model. The two-phase flow field is modeled using the mixed fluid approach in the Eulerian reference frame. A homogeneous equilibrium model has been implemented in the FLACS code to compute the vaporization of the liquid droplets inside the jet. Rain-out is modeled as an effect of jet impingement on the ground. The mass of liquid removed from the jet is transferred to a pool model. The shallow water equations are solved for the pool model and the evaporation rate is estimated from the conservation of enthalpy of the liquid material. The transient pool model is solved simultaneously with the 3D flow field. The flow field is modeled by the Reynolds Averaged Navier-Stokes equations which are closed by the standard k-ε turbulence model. Proper wind boundary conditions are applied by using the Monin-Obukhov similarity theory. This new methodology is used to simulate the Desert Tortoise test series which consisted in four pressurized liquefied ammonia spills.

* *Corresponding author address:* Mathieu Ichard, GexCon AS, Fantoftvegen 38, 5892, Bergen, Norway
+47 40554068, e-mail: mathieu@gexcon.com

2. A MODEL FOR FLASHING RELEASES

In this section we present the methodology developed to assess the hazards of pressurized liquefied gases releases. Before getting into the details of the sub-models and physical phenomenon involved in pressurized liquefied gas releases, we find it useful to define the specific scenarios we are interested in. The material can be stored in different thermodynamic states: vapor, liquid, liquid and vapor. We limit ourselves to the scenarios in which the material is stored as a liquid only. Therefore, the material is either saturated or sub-cooled. A sub-cooled material has a storage temperature lower than the saturation temperature at the storage pressure. In the following, sub-cooled materials are considered.

The first sub-model concerns the computation of the mass flow rate from the storage reservoir and the thermodynamic state of the released material at the rupture plane. The material is stored as a liquid, but it can change phase partially or totally before reaching the exit orifice. Leung (1990) defines low sub-cooling and high sub-cooling conditions based on the storage conditions. If the material is stored upon low sub-cooling conditions, the material flashes before the rupture plane and the flow is two-phase at the exit orifice. For high sub-cooling conditions the material stays in the liquid state until the rupture plane. The parameter η_s allows distinguishing between high and low sub-cooling conditions:

$$\eta_s = \frac{P_{sat}(T_0)}{P_0} \tag{1}$$

The distinction is also based on the parameter $\omega_{t,}$ which is the saturated ω-parameter of the ω-method developed by Leung:

$$\omega = \rho_{l_0} C_p T_0 P_{sat}(T_0)\left(\frac{1}{\rho_{vl_0} h_{vl_0}}\right)^2 \tag{2}$$

In the equations above, the index *0* refers to stagnation conditions inside the reservoir, the index *l* to the liquid phase, *v* to the vapor phase and *vl* to the difference between the vapor and liquid phase. Roughly speaking, if the pressure inside the reservoir is 10% larger than the saturation pressure at the storage temperature, an all liquid release can be expected. Because high sub-cooling conditions were applied in the Desert Tortoise test series, we present only the expression for the mass flow rate for these conditions. The expression for low sub-cooling conditions is discussed in Hanna (2009). For high sub-cooling conditions the mass flow rate is given by a Bernoulli-like expression:

$$G = C_D \sqrt{2\rho_{l_0}(P_0 - P_{sat}(T_0))} \quad (3)$$

The coefficient of discharge is set to C_D=0.6 for liquid releases and the exit pressure is the saturation pressure at the storage temperature; thus phase change occurs outside the reservoir, in the ambient atmosphere.

The saturation pressure at the storage temperature can be several times larger than the atmospheric pressure. At the rupture plane the liquid is also said to be super-heated because its temperature is larger than its normal boiling point. Therefore, a model is needed to simultaneously compute the depressurization of the jet down to atmospheric pressure and the fraction of liquid that flashes. We assume that no air is entrained during the strong expansion of the jet. The equations for the conservation of mass, momentum and energy between the exit plane and the plane where the jet is at atmospheric pressure write (Witlox, 2002):

$$G_e A_e U_e + (P_e - P_{atm}) A_e = G_e A_e U_{atm} \quad (4)$$

$$U_{atm} = U_e + \frac{(P_e - P_{atm})}{G_e} \quad (5)$$

$$H_e + \frac{1}{2}U_e^2 = H_{atm} + \frac{1}{2}U_{atm}^2 \quad (6)$$

From the previous set of equations, termed the 1D expansion model, the velocity, temperature, void fraction and area of the jet can be determined and used to set-up a pseudo-source.

At the positions of the pseudo-source, the CFD computations start. In two-phase flow simulations various treatments of the particle field, in this case the liquid droplets, can be employed. In this work a Eulerian reference frame is used to solve both the continuous and particle field. The Eulerian description of the dispersed phase assumes that the characteristics of the particles (temperature, velocity) can be described as a continuum. Therefore, both the continuous and the dispersed phase are treated with the same computational grid and numerical techniques. We assume that the liquid droplets and gas phase are in local kinetic and thermal equilibrium which means that both phases have the same temperature and velocity. This assumption implies that differences in velocity and temperature between the two-phases are small compared to the variations of these parameters in the overall flow field. Moreover, transport equations for the mass fractions of the material in liquid phase, the material in gas phase and the air are solved so that each control volume has a certain fraction of liquid, vapor and air. This Eulerian method is referred to as the mixed-fluid approach in the literature (Crowe, 2006). The Reynolds Averaged Navier-Stokes equations are solved on a Cartesian grid and the ideal equation of state and the k-ε turbulence model are used to close the system of equations.

The homogeneous equilibrium model has been implemented in the 3D FLACS code in order to account for the processes of droplets evaporation and cooling of the jet. Kukkonen (1994) gives a detailed and comprehensive description of the physics contained in the model. In the homogeneous equilibrium model, it is assumed that the droplets are homogeneously statistically distributed both spatially and in size. From the Dalton's law of partial pressures, the partial pressure of the chemical substance is:

$$P_g = \alpha_g P_{atm} \quad (7)$$

Thermodynamic equilibrium implies that the partial pressure of the chemical, P_g, is the saturation pressure at the mixture temperature. Vapor pressures are computed with the Wagner equation (Poling, 2000). The cooling process can be understood in the following way: as air is entrained inside the jet, the volume fraction of the contaminant vapor decreases (the dilution effect) and so does the vapor pressure. Since the vapor pressure decreases, the mixture temperature must also decrease. The conservation of enthalpy for the mixture of dry air, vapor and liquid droplets must be satisfied as the temperature of the cloud decreases. The conservation of enthalpy can only be achieved if the liquid vaporizes and extract the required amount of latent heat of vaporization to reach equilibrium. When all the liquid has evaporated, air entrainment brings the mixture temperature towards ambient temperature. Ichard (2009) presented a validation study of this model for two-phase flashing jets of propane and butane.

Because the mixed-fluid approach is based on a volume average of both phases, the size and shape of the dispersed phase are not modeled. It means that mean droplet diameters and probabilistic distribution of droplet diameters are not required in the computations. Although it reduces the complexity of the calculations, it poses challenges as regards to the estimation of rain-out. The most common way to predict the amount of rain-out follows this sequence: estimation of a mean droplet diameter and probabilistic density function for droplet diameters, prediction of a critical droplet diameter, computation of the mass of liquid that rains-out as the mass contained in the droplets having a diameter larger than the critical droplet diameter. Information about droplet size and distribution is lacking in the homogeneous model and the approach outlines above can not be used to estimate the rainout. A method based on the trajectories of a horizontal two-phase jet is developed. The method which has been developed and implemented in the 3D CFD FLACS code is illustrated in Figure 1. Rain-out is seen as the resulting effect of jet impingement on the ground.

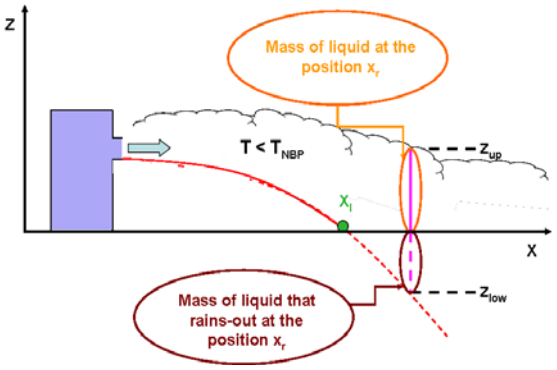

Figure 1 – Jet impingement and rain-out

Some concepts and terms used in this method are now defined. Assume the simplified scenario where the release is in the x-direction and the wind field is aligned with the release direction. For now, in a first step, no obstacles are assumed to be located in the near field of the release. The near field of the release is defined as the region where the liquid droplets have not yet evaporated. The "liquid jet" is the part of the flow field where:

$$T \le T_{sat}(P_{atm}) \tag{8}$$

For each time-step in the 3D computations, the coordinates of the impact point, X_{imp} of the "liquid jet" on the ground are computed. The parabolic trajectory of the liquid jet is calculated and extended downstream of the impact point below the ground (red curve on Figure 1). For each grid point satisfying the conditions:

$$z = z_{ground} \quad x > x_{imp} \quad T \le T_{sat}(P_{atm}) \tag{9}$$

we need to estimate the amount of liquid that rains-out. For such a point, we first compute the mass of liquid which is in the vertical column defined by:

$$z_{ground} \le z \le z_{up} \tag{10}$$

The variable z_{up} is the height of the upper edge of the "liquid jet" (see Figure 1). As a first coarse approximation we assume that the mass of liquid is distributed homogeneously over the vertical column defined by Equation (11).

$$z_{low} \le z \le z_{up} \tag{11}$$

The variable z_{low} is the height of the trajectory below the ground (see Figure 1). The mass that rains-out is the mass of liquid which is in the vertical column defined by:

$$z_{low} \le z \le z_{ground} \tag{12}$$

The predictions of rain-out obtained with this simplified approach will be assessed in the following.

The rain-out is estimated locally and an on-line coupling with a pool model has been implemented. Each rain-out position acts as a source point for the pool model. The spread and vaporization of the liquid is computed simultaneously with the 3D atmospheric wind field. The liquid will spread until it reaches a steady state where the evaporation rate balances the source of mass or obstacles hinder further pool spread. The liquid motion can be described mathematically by the shallow water equations (Toro, 2001). In this work, the shallow water equations are solved on a Cartesian grid:

$$\frac{\partial h}{\partial t} + \frac{\partial h u_i}{\partial x_i} = \frac{\dot{m}_L - \dot{m}_V}{\rho_l} \tag{13}$$

$$\frac{\partial h u_i}{\partial t} + u_j \frac{\partial h u_i}{\partial x_j} = F_{g,i} + F_{\tau,i} \tag{14}$$

The gravity force is given by Equation (15) in which the parameter Δ takes into account, in case of spills onto water, the relative density of water and spilled liquid:

$$F_{g,i} = hg_i \Delta \frac{\partial(h+z)}{\partial x_i} \tag{15}$$

The shear stress between the spill and substrate is given by the general formula:

$$F_{\tau,i} = \frac{1}{8} f_f u_i \left|\overrightarrow{u_i}\right| \tag{16}$$

The transport equation for the specific enthalpy reads:

$$\frac{\partial \theta}{\partial t} + u_i \frac{\partial \theta}{\partial x_i} = \frac{\dot{m}_L}{h}(\theta_L - \theta) + \dot{q}_c + \dot{q}_r + \dot{q}_g + \dot{q}_e \tag{17}$$

The first term on the right hand side is due to the leak, the second is the convective heat transfer, the third is the heat transfer to the pool from radiation, the fourth is the heat transfer to the pool from the substrate, and the last is the heat loss due to evaporation (Melheim, 2009).

The atmospheric boundary layer is modeled by forcing profiles for velocity, temperature and turbulence parameters on inlet boundaries. Wind inlet profiles relays on the Monin-Obukhov length *L* and the atmospheric roughness length z_0. The Monin-Obukhov length can be estimated from measurements and it is positive for stable atmospheric boundary layers, negative for unstable boundary layers and infinity for neutral boundary layers. In risk assessment studies, the Monin-Obukhov length is generally not know and must be guessed, for instance by using the dominant or most hazardous Pasquill stability class and Golder graphs (Bosch, 2005). The inlet velocity profile is logarithmic and can be written as:

$$U(z) = \frac{u_*}{\kappa}\left(\ln(\frac{z}{z_0}) - \psi_m\right) \tag{18}$$

The temperature profile is written as follows:

$$T(z) = T_g + \frac{T_*}{\kappa}\left(\ln(\frac{z}{z_0}) - \psi_H\right) - \Gamma_d z \tag{19}$$

Atmospheric stability effects are accounted for via the Ψ terms. Turbulence profiles on the inlet follow the suggestions of Han (2000).

3. VALIDATION: THE DESERT TORTOISE TEST SERIES

The Desert Tortoise test series consist of four large scale releases of pressurized liquefied ammonia which were performed in the summer of 1983 by the Lawrence Livermore National Laboratory on the Frenchman Flat area of the Department of Energy's Nevada Test Site (Goldwire, 1985). The test site is ideal for conducting dispersion tests both due to the very flat terrain and regular wind patterns. The main objective of the tests was to measure the concentration of ammonia at two distances, 100 m and 800 m downstream of the release point. Ammonia was stored in two 41.5 m^3 capacity highway tanker trucks which were connected to a spill line with an orifice plate at the end. Ammonia was self-pressurized in the tanker trucks and additional nitrogen gas was used to maintain a constant pressure inside the tankers to obtain a constant flow rate. The exit orifice was 0.79 m above the ground and was specially designed such that the ammonia remained liquid until the end of the spill line. In addition to measurements of gas concentration, the temperature was recorded at several positions. Three thermocouples were placed on the ground surface along the center line of the jet at distances of 3 m, 5 m and 9 m from the exit orifice. These thermocouples provided information on possible rain-out and formation of a liquid pool. The temperature was also recorded at the same position as the gas concentrations. Gas concentrations and temperature were measured at heights of 1 m, 2.5 m and 6 m for the 100 m row and 1 m, 3.5 m and 8.5 m for the 800 m row. Eleven meteorological stations were used to evaluate the parameters of the atmospheric boundary layer over the test area

The models presented in Section 2 are now evaluated against the experimental data. For the four tests DT1, DT2, DT3, and DT4, the storage pressure was more than 10% larger than the saturation pressure at the storage temperature. We therefore expect the material to be in the liquid phase at the exit orifice. The mass flow rates are calculated with Eq.(3) and the results are reported in Table 1. The predictions globally over-predict the measurements by 12-13% which is found to be acceptable.

Test	P_0 [bar]	$P_v(T_0)$ [bar]	Mass Flow Rates [kgs^{-1}]		
			Predicted	Measured	Error
DT1	14.6	9	90.9	79.6	-13%
DT2	15.1	8.5	126.2	111.4	-12%
DT3	15.2	9.3	119	133.1	11%
DT4	15	10	109.9	96.6	-13%

Table 1 – Mass flow rate predictions

The expansion model, i.e. Eqs. (4), (5) and (6), is used to evaluate the properties of the pseudo-source. In the computations the experimental mass flow rates have been used. In Table 2 we give the characteristics of the pseudo-source for the test DT2. The temperature, velocity and area of the jet at ambient pressure, U_{atm} and A_{atm}, and the mass fraction of vapor are used to set-up the pseudo-source in the 3D FLACS code. We note that the velocity is increased by almost a factor 4 and that the area of the jet is increased by a factor 40 due to the generation of vapor during the flashing process. The kinetic term in the expression giving the mass fraction of vapor, Eq.(6), can be neglected in this case as it is two orders of magnitudes smaller than the thermodynamic term.

T [K]	U_e [ms^{-1}]	U_{atm} [ms^{-1}]	A_e [m^2]	A_{atm} [m^2]	X_g [-]
-33.5	23.3	86.3	0.007	0.267	0.18

Table 2 – Pseudo-source parameters

The 3D computations with the CFD are now discussed; the predictions of the amount of rain-out, pool spreading and vaporization are evaluated. First, sensitivity studies on the grid resolution have been performed to investigate the effects of the resolution in the z-direction on the predicted amount of rain-out. Two different resolutions have been tested. The coarse resolution had a grid size of 0.18 m with 5 grid cells below the release point. The fine resolution had a size of 0.09 m with 10 grid cells below the release point. The coarse resolution gave 15 % rain-out more than the fine resolution. A 15 % difference is found to be acceptable when the resolution is divided by two. The coarse resolution has been used in the simulations. In the x-direction the minimum grid cell size was 0.5 m in the very near field of the release (region of impingement of the "liquid jet" on the ground) and 2 m elsewhere. In the y-direction, the minimum grid cell size was 0.18 m around the leak and it was gradually increased to 2 m. In the experiments the amount of rain-out has been deduced form the estimations of the mass fluxes trough the first row of sensors 100 m downwind of the spill point. The mass fluxes were integrated over the duration of the spills and the difference between the mass spilled and the integrated mass fluxes at the 100 m row gave the amount of rain-out. Table 3 shows the predicted and observed amounts of liquid that rains-out on the ground for each test. The simulations tend to over-predict the amount of rain-out by 20-30 %, except for DT1 where an over-prediction of a factor of two is seen. This over-prediction can be explained, in part, by the fact that in the experiments the integration with time of the mass fluxes has been performed over the whole release duration. It could be that some ammonia that had rained-out, also had evaporated and been transported by the flow field to the 100 m row within the duration of the release. Then some of the gas evaporating from the pool has been taken into account in the integration of the mass fluxes, thus decreasing the amount of rain-out. Moreover, the test area was covered by water during the night before the release or even during the release (DT1 and DT2). The ground had then a high level of humidity, perhaps saturated with water and these conditions might have increased the vaporization rate of the pool, reinforcing the previous observation.

Test	Rain-out [% of mass spilled]	
	Observed	Predicted
DT1	20 %	43 %
DT2	36 %	43 %
DT3	39 %	45 %
DT4	30 %	40 %

Table 3 – Rain-out predictions

Finally, we present 2D snapshots of the pool depth for the test DT1 showing the development of the pool due to the rain-out. The first snapshot, 20 s after start of release, shows an elongated shape for the pool because the liquid that had just rained-out did not have time to spread much yet. The first snapshot can be seen as an approximation of the rain-out footprint. As time increases the liquid spreads and the shape of the pool tends towards a circular shape. After the end of release, at 126 s, the pool vaporizes and gradually disappears.

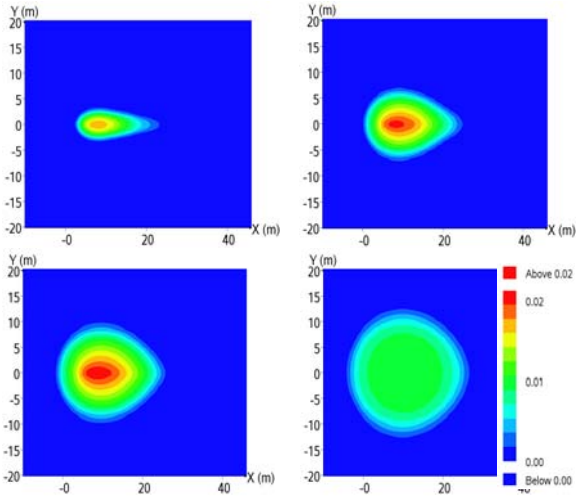

Figure 2 – Pool Depth, DT1, times after start of release: [Upper left] t=20s, [Upper right] t=60s, [Lower left] t=100s, [Lower right] t=160s

Figure 3 shows the plume for the test DT2, 1 m above the ground 250 s after the release started. The sensors at the 100 m row and 800 m row are also shown. The vapor evaporated from the pool can be seen in the near field.

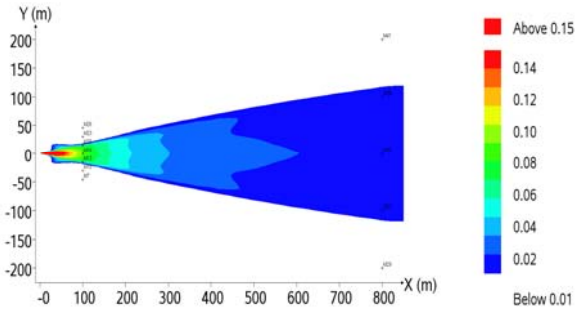

Figure 3 – Plume for DT2, 250s after start of release and 1m above the ground

Predictions of gas concentrations are now evaluated. Firstly, the maximum concentrations predicted at the rows 100 m and 800 m at the two first heights are compared with the observations. An averaging time of 15 s has been used for the experimental time series. This averaging time has been set so that the short time peaks, puffs, of concentrations due to turbulence intermittency in the atmospheric boundary layer were averaged out as the RANS turbulence model k-ε is not able to predict such a characteristic of the turbulence. Statistical Performance Measures (SPM) have been computed with 16 values. The expressions for the SPM are given below:

$$MRB = \left\langle \frac{C_{obs} - C_{pred}}{0.5\left(C_{pred} + C_{obs}\right)} \right\rangle \quad (20)$$

$$MRSE = \left\langle \frac{\left(C_{pred} - C_{obs}\right)^2}{0.25\left(C_{pred} + C_{obs}\right)^2} \right\rangle \quad (21)$$

$$MG = \exp\left\langle \ln\left(\frac{C_{obs}}{C_{pred}}\right) \right\rangle \quad (22)$$

$$VG = \exp\left\langle \left(\ln\left(\frac{C_{obs}}{C_{pred}}\right)\right)^2 \right\rangle \quad (23)$$

MRB stands for Mean Relative Bias; MRSE for Mean Relative Square Error; FAC2 is the fraction of predictions within a factor of two of the observations; MG is the Geometric Mean bias and VG the Geometric Variance. The SPM must provide a measure of the tendency of the model to over-predict or under-predict the observations and a measure of the level of scatter from the average over/under-prediction. Each of the SPM has some advantage and inconvenient, we refer to Ivings (2007) for more details. Table 4 shows the values of the SPM for our simulations:

FAC2	**0.94**
MRB	**-0.25**
MRSE	**0.11**
MG	**0.77**
VG	**1.12**

Table 4 – SPM values applied to maximum concentrations at the rows 100m and 800m for the two first measurement heights.

The results obtained are satisfying; an over-prediction of around 25 % and a low level scatter are seen. The over-prediction noted in the SPM values is mainly due to the predictions at the 100 m rows at the height of 1 m. Point-wise comparisons are needed for a further investigation of the performance of the model.

Profiles of concentration 100 m downwind 1 m above ground for the tests DT1 and DT3 are shown on Figure 4. The sensor on the axis of the release is considered (sensor G05 in the experiments). The plots can be divided in two parts. The first part corresponds to the concentration observed over the duration of the release. An over-estimation of around 30 % is observed for both plots. At 100 m downwind the momentum of the jet has not totally dissipated yet and the concentrations are still mainly influenced by the source conditions. Therefore, the over-estimation is believed to be due to a too low mixing in the turbulent two-phase jet. The second part starts around 180 s for DT1 and 200 s for DT3. The release has stopped and the concentration recorded comes from the vaporization of the NH_3 pool. This phenomenon is observed both in the simulations and the experiments. Gas is still present 300-400 s after the end of release in a non-negligible quantity. The over-prediction of concentrations for DT1 is certainly due to the over-estimation of rain-out (see Table 3) but could also be due to the representation of atmospheric meandering flows. Although we are still at 100 m downwind, the dispersion of NH_3 is now controlled by atmospheric turbulence. It could be that due to the meandering the plume coming from the pool has missed the sensor. The two plots on Figure 5 show the concentration at a height of 2.5 m at the row 100 m at the same sensor as for the height 1 m, for the tests DT1 and DT3. The over-estimation seen

at the height 1 m is not observed at the height 2.5 m because the source effects have been dissipated or at least are less important than at the height 1 m.

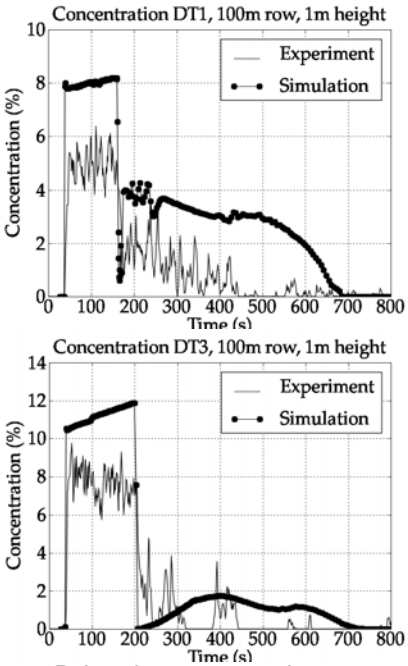

Figure 4 – Point-wise concentration comparisons for DT1 and DT3 at the sensor G05, height 1m

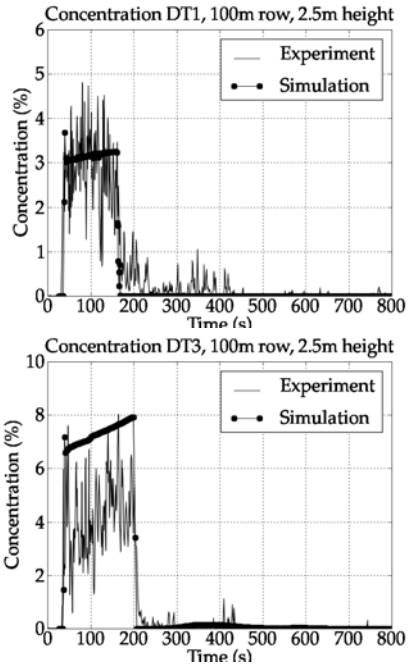

Figure 5 – Point-wise concentration comparisons for DT1 and DT3 at the sensor G05, height 2.5m

Predictions of concentration 800 m downwind of the release point are very satisfying as it can be seen on Figure 6. The profiles are at a height of 1 m, sensor G22 for the test DT2 and sensor G21 for DT4. At 800 m the dispersion is totally controlled by atmospheric turbulence, all source effects have dissipated.

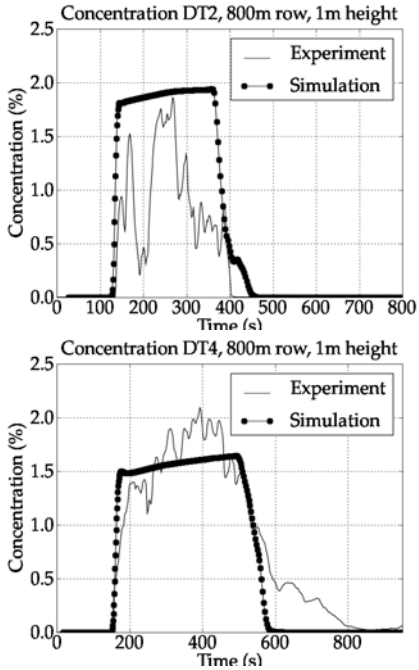

Figure 6 – Point wise concentration comparisons for DT2 and DT4 at the 800m row, height 1m

Temperatures have also been measured in the test series. Figure 7 presents a comparison between predicted and observed temperature profiles for DT1 and DT3 at a height of 1 m and 100 m downwind. The sensor is the same sensor than for the concentration plots. Temperature profiles give information on the presence or not of liquid droplets. As the temperature is larger than the normal boiling point of ammonia, all the liquid droplets have evaporated before the 100 m row. An over-estimation of the decrease in temperature is seen and is certainly due to the over-estimation of the concentration as discussed previously.

4. CONCLUSION

A methodology to perform 3D CFD computations of pressurized liquefied gas releases has been developed and presented. The method has been implemented in the CFD model FLACS. The whole chain of events occurring in pressurized liquefied gas releases is modeled. The source term after flashing is estimated by using a 1D expansion model. The

parameters of the jet given by the 1D expansion model are used to set-up a pseudo-source in the 3D FLACS code. The 3D calculations start at the pseudo-source position. The dispersion of the two phase jet, the rain-out, the pool spreading and evaporation are computed by the CFD code.

The methodology has been used to simulate the Desert Tortoise test series conducted by the Lawrence Livermore National Laboratory. The four large-scale releases of pressurized liquefied ammonia have been simulated. Rain-out was estimated during the experiments and the predictions of the CFD model are within 30 % of the observations for three of the four tests. Statistical Performance Measures have been used to assess the performance of the model in predicting maximum gas concentrations at the rows 100 m and 800 m downwind of the release point. An over-prediction of 25 % is seen and 94 % of the predictions are within a factor of two of the observations. Point wise comparisons of gas concentrations and temperature have also been reported. The point-wise comparisons of gas concentrations show the increase of the hazard duration due to the rain-out process.

Future work will include the presence of obstacles in the near field of the two-phase jet, an improvement of the rain-out model and a detailed investigation of the representation of turbulence mixing inside the two-phase jet.

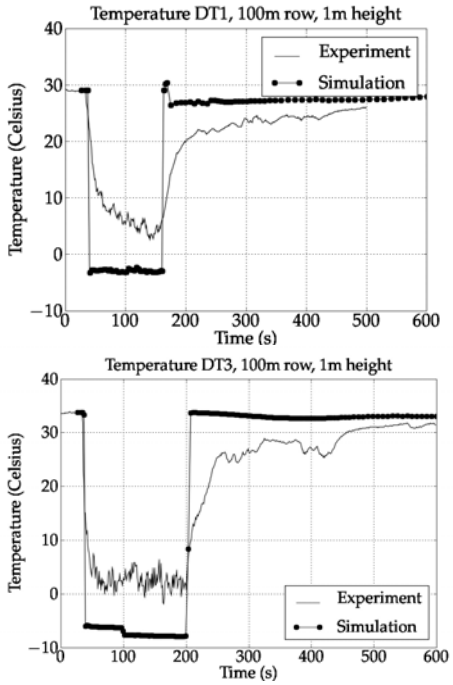

Figure 7 – Point-wise temperature comparisons for DT1 and DT3 at the sensor G05, height 1m

5. ACKNOWLEDGEMENTS

This research has been sponsored by a PhD grant of the Norwegian Research Council. The authors would also like to acknowledge the StatoilHydro travel fund.

6. REFERENCES

Bosch, C. J. H. van den, Weterings, R. A. P. M. (Ed), 2005: Methods for the calculation of physical effects – due to releases of hazardous materials, CPR 14E. (TNO Yello Book) 3rd edition, 2nd print, TNO, The Hague, The Netherlands

Crowe, C.T (Ed), 2006: Multiphase Flow Handbook, Taylor & Francis Group, ISBN 0-8493-1280-9

Han, J., Arya, S. P., Shen, S., Lin, Y.-L., 2000: An estimation of turbulent kinetic energy and energy dissipation rate based on atmospheric boundary similarity theory. Tech. Rep. CR-2000-210298, NASA, USA

Hanna, S., Britter, R., Leung, J., Weil, J., Sykes, I, 2009: Toxic Industrial Chemicals (TIC) Source Emissions Model Improvements, prepared by Hanna Consultants, prepared for Defense Threat Reduction Agency Joint Science and Technology Office, Report Number P098-4

Ichard, M., Hansen, O. R. and Melheim, J. A., 2009: Modeling of flashing releases around buildings, 90th AMS annual meeting, Phoenix, AZ, USA

Ivings, M.J., Jagger, S.F., Lea, C.J. and Webber, D.M., 2007: Evaluating Vapor Dispersion Models for Safety Analysis of LNG Facilities Research Project, Health & Safety Laboratory

Kukkonen, J., Kulmala, M., Nikmo, J., Vesala, T., Webber, D.M., Wren, T., 1994: The homogeneous equilibrium approximation in models of aerosol cloud dispersion. *Atmos. Environ.* Vol. **28**, No. 17, pp. 2763-2776

Leung, J.C, 1990: Two-phase flow discharge in nozzles and pipes – a unified approach. *J. Loss Prev. Process Ind.*, Vol. **3**, pp. 27-32

Melheim, J. A., Ichard, M. and Pontiggia, M., 2009: Towards a computational fluid dynamics methodology for studies of large-scale LNG releases, Hazards XX1, paper 115, Manchester, UK

Poling, B.E., Prausnitz, J.M., O'Connell, J.P., 2000: The properties of gases and liquids, fifth edition. *McGraw-Hill Professional*, ISBN 00-701-1682-5

Toro, E. F., 2001: Shock-capturing methods for free-surface shallow water flows. Wiley, UK

Witlox, H. W. M. and Bowen, P.J., 2002: Flashing liquid jets and two-phase dispersion, Health & Safety Executive, 403/2002